## Geometric characterization of SARS-CoV-2 pandemic events

Ivan Bonamassa, <sup>1,\*</sup> Marcello Calvanese Strinati, <sup>1</sup> Adrian Chan, <sup>1</sup> Ouriel Gotesdyner, <sup>1</sup> Bnaya Gross, <sup>1</sup> Shlomo Havlin, <sup>1</sup> and Mario Leo<sup>2</sup>

<sup>1</sup>Department of Physics, Bar-Ilan University, 52900 Ramat-Gan, Israel <sup>2</sup>Dipartimento di Matematica e Fisica "Ennio de Giorgi", Università del Salento, Lecce, Italy (Dated: July 22, 2020)

While the SARS-CoV-2 keeps spreading world-wide, comparing its evolution across different nations is a timely challenge of both theoretical and practical importance. The large variety of dissimilar and country-dependent epidemiological factors, in fact, makes extremely difficult to understand their influence on the epidemic trends within a unique and coherent framework. We present a geometric framework to characterize, in an integrated and low-dimensional fashion, the epidemic plume-like trajectories traced by the infection rate, I, and the fatality rate, D, in the (I,D) plane. Our analysis enables the definition of an epidemiometric system based on three geometric observables rating the SARS-CoV-2 pandemic events via scales analogous to those for the magnitude and the intensity of seismic events. Being exquisitely geometric, our framework can be applied to classify other epidemic data and secondary waves, raising the possibility of designing epidemic alerts or early warning systems to enhance public and governmental responses to a rapidly emerging outbreak.

The unprecedented amount of epidemic data collected worldwide on SARS-CoV-2 raises nowadays a unique opportunity to quantify, in a way analogous to other extreme events [1, 2], the catastrophic impact that a pandemic can have on the globalized world [3, 4]. In the context of earthquakes, for example, the existence of the Richter [5] and Mercalli [6] measures, quantifying respectively the magnitude and the intensity of a local seismic event, has helped policy-makers to take informed decisions yielding better intervention strategies (e.g. by means of tsunami alerts or rapid post-earthquakes notifications [7–10]) and strong governmental actions (e.g. investments in anti-seismic infrastructures [11, 12]) to prevent their potential impact. Similarly, in meteorology, the Fujita [13] and the Saffir-Simpson [14, 15] scales have offered researchers with heuristic measures to estimate the potential damage inflicted by, respectively, tornados and hurricanes on human-build structures and vegetation, raising the opportunity of designing everincreasingly refined early warning systems and alert protocols [16–18]. In the realm of pandemics, however, metric systems enabling a comprehensive classification of their types have (to the best of our knowledge) never been proposed, resulting in a fundamental gap in the human fight against this type of catastrophic events.

The theoretical and practical implications of this important and timely challenge are numerous. Disposing of a robust and comprehensive framework to classify the SARS-CoV-2 pandemic events reported across different countries not only can enhance early [19, 20] public and governmental responses in containing the spreading and/or better absorbing the impact of a rapidly emerging epidemic outbreak, but it can further provide new information to better understand real-world epidemics and to boost the forecasting power of existing models [21–29].

A fundamental difficulty to achieve this goal relies in the large heterogeneity of epidemiological and country-dependent factors characterizing the global pandemic trends. Diverse isolation [30] and social distancing strategies [31–39], age, gender impact [40, 41] and demographic characteristics of different populations [42], local transportation systems [43–47], tracking and testing policies [48, 49], health systems' capacities [50] and many other factors, make difficult the design of quantitative epidemiometric systems for country-to-country comparison [51–53]. Moreover, epidemic models or inference algorithms fine-tuned to this constellation of features, inevitably result into theoretical or semi-empirical frameworks whose complexity rapidly increases with the large number of data-driven parameters considered [23, 54–61].

In this work, we present a geometric, low-dimensional method to classify the impact the SARS-CoV-2 pandemic events observed across different nations. After performing a statistical best-fit of the epidemic data for the infected, I, and deceased, D, rates, we analyze the geometry of their plume-like trajectories in the (I, D)plane. Moving to a polar representation, we classify the plumes' form through a set of three geometric parameters vielding two complementary rating scales for the SARS-CoV-2 pandemic types: one according to their *epidemic* magnitude—labeled with roman numbers from  $\mathbb{I}$  to  $\mathbb{X}$ for increasing strengths—and measuring the "size" of a national outbreak, and a second one according to their intensity—labeled alphabetically from A to D for increasing speed—quantifying instead the damage inflicted on the population. Even though each country exhibits its own pandemic fingerprint, our geometric method unveils hidden similarities shared by their global trends emerging from an integrated representation of their evolution. We further provide a qualitative understanding of the epidemiological information contained in the developed epidemic measures, and discuss the theoretical and practical implications of our results.

1. Comparing the pandemic trends. To set the stage

<sup>\*</sup> ivan.bms.2011@gmail.com

for a cross-comparison of the countries' pandemic trends, let us consider two widely reported epidemiological observables, i.e. the infected (I) and the fatality (D) daily rates. These quantities can vary strongly from one country to another, depending on a wide variety of factors. Even within the same country, the numbers may fluctuate from one day to another due to delays in reporting, transitions to new surveillance and/or tasting systems, or simply because of weekly periodic variations in the number of daily tests performed. Smoothening the data under a suitable moving average window unveils the trends of the time series, enabling a preliminary comparison.

As a demonstrative example, let us consider the pandemic trends reported in Italy and in Germany (Fig. 1). In both countries, it took approximately 6 weeks for the outbreaks to reach their infection peaks, with similar fast-rising trends and comparable numbers of newly infected patients per day. Their post-peak behaviors, however, differ noticeably: whereas Germany's infection curve has decayed almost as quickly as it rose, resulting in a reduction by 50% of the daily infected in nearly 15 days, it has taken almost double this time to Italy to reach similar conditions. This is nicely reflected in the values of the skewnesses calculated after best-fitting the data with asymmetric Gaussians (Fig. 1, legend), showing a decay of the Italian trend roughly 2.3 times slower than the one observed in Germany. Slow infection rate decays similar to those reported in Italy have also been observed in the United States, the United Kingdom or Russia and can be explained as the result of new regional outbreaks spreading throughout the country after the national lockdown, hinting at a difficulty in identifying/containing the virus since its early stages. Additional information can be found by performing a similar analysis of the fatality rates. This quickly reveals that Italy had to face much

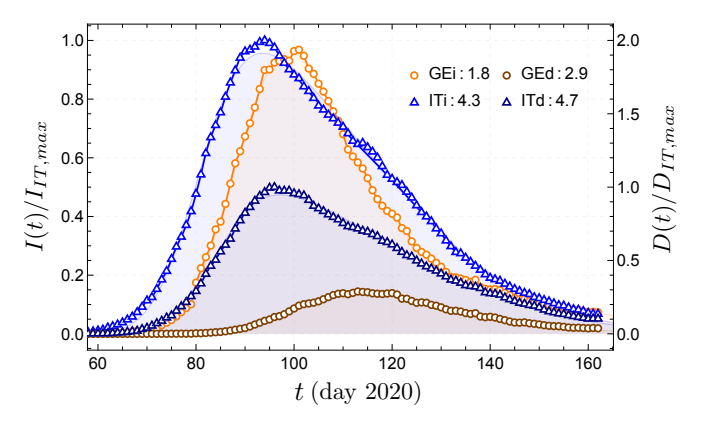


FIG. 1. Temporal evolution of epidemic profiles. (Color online) Comparison between SARS-CoV-2 infected and fatality rate profiles for Italy (respectively, blue and dark blue triangles) and Germany (respectively, orange and dark orange circles) under a 15-days moving average. Infected and deceased rates have been normalized with respect to the corresponding largest values reported in Italy. Different y scales have been chosen for clarity of exposition. (Legend) Skewnesses values obtained after best fitting the global trends via skewness Gaussian distributions. Data taken from Ref. [62].

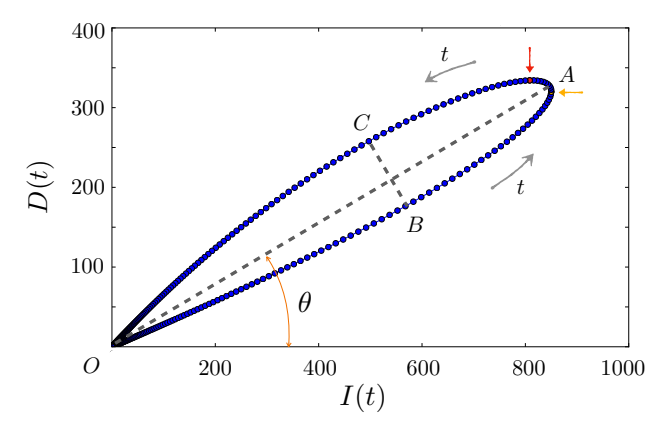


FIG. 2. Geometric parametrization of typical epidemic trends. (Color online) Demonstration of our geometric method to analyze a typical epidemic trajectory in the (I,D) plane; in this representation, time flows counterclockwise. Yellow and red arrows point respectively at the infected and fatality rate peaks, while the markers evolve on a daily rate. We calculate the largest radius,  $r_{max} \equiv \overline{AO}$ , its inclination,  $\theta$ , and the largest width,  $r_{\perp} \equiv \overline{BC}$ , of the plumelike trajectory traced by the epidemic evolution. These quantities define the triple  $(r_{max}, \theta, \rho)$ , with  $\rho \equiv r_{\perp}/r_{max}$ , used to analyze classify events as described in the text.

more critical conditions, counting (on average) at least 3 times more fatalities per day than Germany, with a death peak located only 4 days after the infected one (by contrast with the 2 weeks lag reported in Germany) and a skewness roughly twice the one measured based on the German data (Fig. 1, legend). By looking at these differences separately, one can heuristically conclude that both countries have experienced outbreaks with similar magnitudes though causing very different damages on the population, with Germany applying a more efficient policy of containment and/or testing and with Italy reaching very critical level in its health system.

To extend the comparison to other countries, it proves essential to identify a suitable metric system grasping and systematically quantifying the relevant information (e.g. peak values, infected-fatality peaks lags, post-peak decay rates, etc.) enshrined in the evolution profiles of the I and D trajectories. In the spirit of dynamical systems theory [63], we approach this problem by departing from the representation of the dynamical observables I(t)and D(t) as functions of time, focusing instead on their mutual evolution in the (I, D) plane (Fig. 2). In this way, a comprehensive portrait of the outbreak dynamics of each country can be described by an integrated plumelike trajectory (Fig. 2) whose geometric features, as we shall see in what below, provide an exhaustive and lowdimensional classification of the SARS-CoV-2 pandemic types according to their magnitude and intensity.

2. Geometric parametrization. In the (I, D) plane, the daily epidemic state of each country traces a trajectory that, after departing from the healthy phase (0,0), leaves behind its own epidemic fingerprint. For reasons that will be clarified below, let us call "typical" an epidemic trajectory analogous to the one depicted in Fig. 2

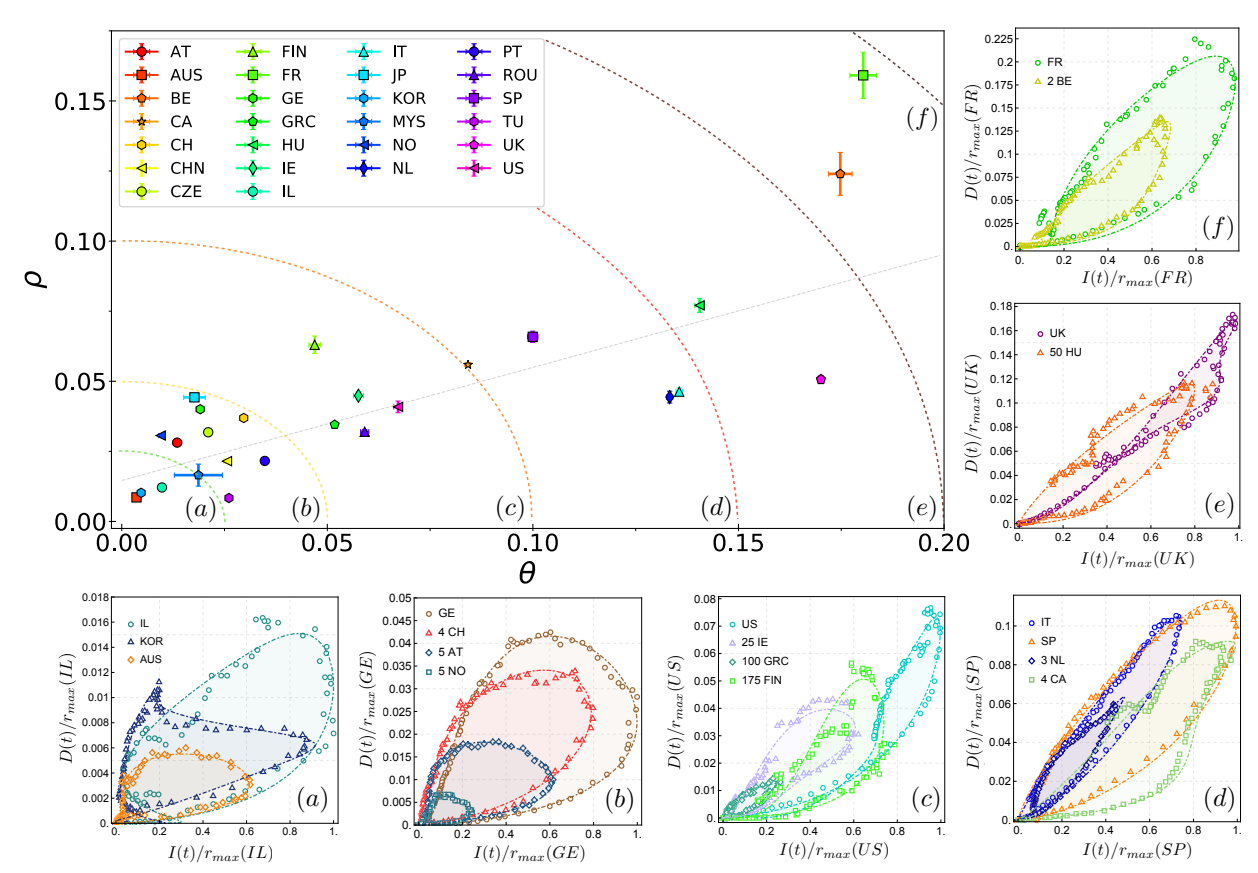


FIG. 3.  $(\theta, \rho)$ -parametrization of typical SARS-CoV-2 pandemic trajectories. (Color online) a)-f) Epidemic trajectories (dot-dashed curves) in the (I, D) plane obtained by interpolating the fitted epidemic states of each country describing their first-wave events. These are generated via the distribution functions best fitting the infected and fatality rates (as in Fig. 1) ruling the evolution of the real-world epidemic states (markers). The  $(\theta, \rho)$  phase diagram summarizes the results of our geometric analysis, where error bars are calculated by considering a confidence interval of 99% over values of  $\theta$  and  $\rho$  for trajectories fitting epidemic data under moving n-day averages with n from 1 to 15. A linear regression analysis yields  $\rho \simeq \rho_0 + \alpha \theta$ , with intercept  $\rho_0 = (1.5 \pm 0.5) \times 10^{-2}$  and slope  $\alpha = 0.40 \pm 0.06$  (dashed gray line). The linear dependence of  $\rho$  on  $\theta$  is supported by a Pearson coefficient  $\tilde{r} \simeq 0.81$  [64]. Countries in the scatter plot are then selected according to shells (dashed circles) of increasing radiuses, identifying six heuristic regimes, ranging from a) the ideal scenario of slow outbreaks with good tracking intervention and low fatality rates, to f) extreme cases representing very fast outbreaks with high case-fatality rates and critical conditions of their health systems. a)-f) Sampled trajectories belonging to each heuristic group exhibit epidemic angles (notice the different extend of the y-axes) whose similarities can be better highlighted by normalizing the epidemic data of each group via the largest  $r_{max}$  of the country in the collection. The normalization factors are respectively: a)  $r_{max}(IL) \simeq 5.2 \times 10^2$ , b)  $r_{max}(GE) \simeq 5 \times 10^3$ , c)  $r_{max}(US) \simeq 3 \times 10^4$ , d)  $r_{max}(SP) \simeq 7 \times 10^3$ , e)  $r_{max}(UK) \simeq 5.3 \times 10^3$ , f)  $r_{max}(FR) \sim 4.2 \times 10^3$ .

and characterized by a dynamics that unfolds counterclockwise in the plane, reaching first the infected peak, then the fatality peak, and finally heads back towards the axes origin. Notice that during this heading back regime, new outbreaks could emerge due to e.g. premature lifting of the lockdown measures, pushing the epidemic state to trace a different plume-like trajectory (Fig. 9a) describing a new epidemic event. Here, we focus our analysis on the epidemic data reported during the first-wave events in countries that have passed both their infected and fatality rate peaks. In the discussion section we will see how our geometric method can be naturally extended to analyze second-wave events like those observed in United States, Iran or Israel (see Fig. 9b).

To quantitatively compare the countries' typical epidemic trajectories, we introduce three geometric parame-

ters,  $(r_{max}, \theta, \rho)$ , that we measure after transforming the epidemic observables I, D into polar coordinates. We define with  $r_{max}$  the maximal radius of the epidemic trajectory, with  $\theta$  the angle formed by  $r_{max}$  with respect to the I-axes, and finally with  $\rho = r_{\perp}/r_{max}$  the relative width of the plume-like curve, where  $r_{\perp}$  is its maximal width (Fig. 2). While  $r_{max}$  measures the largest extent of the epidemic plume—and has therefore units of population—the quantities  $\theta$  and  $\rho$  have a genuine geometric nature and disclose different information about the *intensity* of an epidemic event. Large values of  $\theta$ , in fact, reflect a fast raise of the number of fatalities jointly with a rapid increase of the newly infected, which would occur in cases of a critical health system but also reflect the country's demographic features, like age and morbidity distributions, social interactions, etc. In this respect,

we adopt  $\theta$  as an estimator of the epidemic "speed". with large (small) angles describing fast (slow) outbreaks. The parameter  $\rho$ , on the other hand, can be written in terms of the "eccentricity", e, of the epidemic trajectory as  $\rho = \sqrt{1 - e^2}$  [65], so that decreasing values of  $\rho$  characterize narrower plumes. This would naturally reflect situations of rapid patient identification, resulting in lower critical conditions of the country's hospitals and hence to less fatalities, i.e. lower values of the angle  $\theta$ . The results in Fig. 3 support this heuristic interpretation, disclosing a linear relation between the two geometric observables  $\theta$  and  $\rho$ . In light of the latter, we have selected countries according to their Euclidean distance from the origin of the  $(\theta, \rho)$  scatter plot, yielding a preliminary partitioning of their outbreaks according to their speed, as shown in Fig. 3 a)-f). Besides highlighting similar inclination of the epidemic trajectories, the normalization by  $r_{max}$  adopted in Fig. 3 a)-f) further discloses an additional degree of similarity between countries based on the time lag separating infected and fatality rate peaks. Countries with low angles like e.g. Germany, Austria or Norway (Fig. 3b) feature, in fact, round plumes with well separated peaks as well as more narrow forms like those reported in e.g. Israel (Fig. 3a), Greece or Finland (Fig. 3c). On the contrary, countries with large epidemic angles always correspond to narrow plumes with strong peak-to-peak proximity, as observed e.g. in Italy (Fig. 3d), Hungary (Fig. 3e) or Belgium (Fig. 3f). As we shall see in the next section, the eccentricity of the normalized epidemic plumes nicely grasps this important information, enabling to define a simple vet informative metric system characterizing the intensity of the SARS-CoV-2 types.

Before delving into the details of this classification, let us complete the picture by considering those epidemic plumes which have not been included in the analysis due to their *non-typical* evolution in the (I, D) plane. This includes epidemic data describing first-wave events whose fatality rate peak has preceded the infected one, as ob-

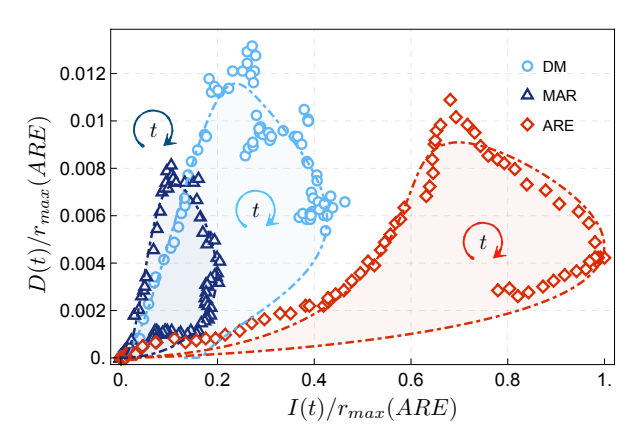


FIG. 4. Non-typical SARS-CoV-2 trajectories. (Color online) Epidemic trajectories featuring clockwise evolution, due to a fatality peak preceding the infected one, as reported in Morocco, United Arab Emirates (ARE), Iran, Dominican Republic and other countries. Here,  $r_{max}(ARE) \simeq 3.2 \times 10^2$ .

served e.g. in Brazil, Mexico, United Arab Emirates, Iran (Fig. 4) and few others. Such peak inversion translates into a clockwise evolution of the epidemic trajectory in the (I,D) plane, whose geometric features could, in principle, be analyzed according to our developed method but should not be similarly interpreted. Fatality-rate peaks preceding the infected ones can be, in fact, only explained as the result of sparse and incomplete reporting due to e.g. limited resources at early stages of diagnostics or absence of post-mortem identification. For the sake of simplicity, in what follows we will focus only on the analysis of typical epidemic trajectories, while the classification of non-typical cases will be performed elsewhere.

3. Classification of SARS-CoV-2 types. Having introduced a geometric parametrization of the countries typical epidemic trajectories, let us now focus on defining a suitable and conventional metric system to systematically quantify their magnitude and intensity.

Outbreak magnitude. As we anticipated, the parameter  $r_{max}$  yields an integrated measure in the (I, D) plane of the largest extent of an epidemic trajectory in units of population, offering the opportunity to analyze the dependence of the epidemic extent on the population size, P, of the country where it spread. By plotting the distribution of  $r_{max}$  as a function of P (Fig. 5), we find an approximate power law  $r_{max} = AP^{\beta}$ , with  $A \in (0,1)$  a country-dependent proportionality factor and  $\beta$  an exponent close to one. The nearly linear relation can be explained by interpreting A as the largest fraction of daily infected and deceased reported for a given population size, suggesting a rudimentary yet informative scale to meaningfully quantify the epidemic magnitude of each country. To this aim, let us introduce the dimensionless parameter  $\chi = \log r_{max} / \log P$ . Because  $r_{max}$  and P are linearly proportional, this relation reads as

$$\chi = 1 + \log \mathcal{A} / \log P,\tag{1}$$

where P>1, so that  $\chi\in(-\infty,1)$  is a monotonically increasing function of the proportionality factor  $\mathcal{A}\in(0,1)$ . This fraction is bounded by two extreme cases:  $\mathcal{A}\to 0$  describing an extremely weak (nearly absent) outbreak with only few infected/deceased daily cases, and  $\mathcal{A}\to 1$  representing instead the unlikely event of a nearly full population infected/deceased in a single day. Similar to the Richter metric system for local seismic events, an epidemic magnitude scale can be conventionally defined by choosing a suitable, monotonically increasing function of  $\chi$  in Eq. (1), where  $\chi$  can be interpreted as the "epidemic force" of an outbreak, measuring the largest fraction of new infected and deceased reported in a single day. Let us therefore define the epidemic magnitude as

$$\mathcal{T}(\chi) = 10^{\chi/\chi^*},\tag{2}$$

where  $\chi^* \equiv 1 - 3/\log P$  plays the role of a characteristic epidemic strength. The choice of  $\chi^*$  allows to assign the scale  $\mathcal{T} = 10$  to a pandemic event with nearly 0.1%

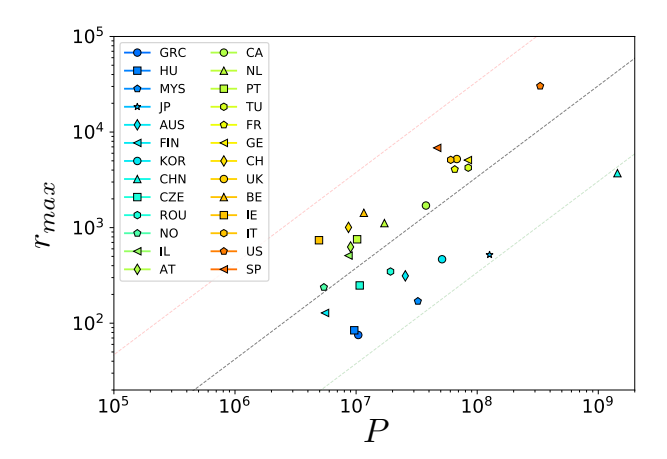


FIG. 5. Extent/population correlation in SARS-CoV-2 trajectories. (Color online) Distribution of  $r_{max}$  vs. population size, P, for the countries listed in Fig. 3. A linear fit  $(p\text{-value} \sim 10^{-6})$  yields  $\log(r_{max}) = r_0 + \beta \log(P)$ , with intercept  $r_0 = -4.1 \pm 1.5$  and slope  $\beta = 0.95 \pm 0.20$  (dashed gray line). The statistical significance of the linear relation is further supported by a Pearson correlation coefficient  $\tilde{r} \sim 0.71$ . Data points are are colored from blue to red for increasing values of the epidemic magnitude  $\mathcal{T}$  (see Tab. I). Dashed green and red lines respectively describe the boundary of the ++ and -- categories, rating the efficacy of each country intervention strategies (we refer to the main text for details).

of the population reported infected and/or deceased in a single day (i.e.  $\mathcal{A}^* = 10^{-3}$ ), an outcome of catastrophic proportions. In light of Eqs. (1)–(2), we introduce an epidemiometric system classifying epidemic events by increasing magnitudes that is described as follows:

- I)  $T \in [0.0, 0.9]$ , micro events: very weak outbreaks having strengths  $\chi < 0$  or, equivalently,  $r_{max} < 1$ , i.e. an average of less than 1 infected case per day;
- III)  $T \in [1.0, 1.9]$ , minor events: weak outbreaks with non-negative strengths corresponding to values of  $r_{max} \in [1, 4)$  for small countries with  $P \sim 10^5$ , and  $r_{max} \in [1, 32)$  for large countries with  $P \sim 10^8$ ;
- III)  $T \in [2.0, 2.9]$ , light events: epidemics featuring e.g. values of  $r_{max} \in [4, 9)$  if  $P \sim 10^5$ , and  $r_{max} \in [32, 250)$  for large countries with  $P \sim 10^8$ ;
- IV)  $T \in [3.0, 3.9]$ , mild events: outbreaks characterized by e.g.  $r_{max} \in [9, 16)$  if  $P \sim 10^5$ , and  $r_{max} \in [250, 10^3)$  if  $P \sim 10^8$ ;
- V)  $\mathcal{T} \in [4.0, 4.9]$ , moderate events: epidemics with e.g.  $r_{max} \in [16, 25)$  for  $P \sim 10^5$ , and  $r_{max} \in [10^3, 3 \times 3.1 \times 10^3)$  for  $P \sim 10^8$ ;
- VI)  $T \in [5.0, 5.9]$ , strong events: epidemics with e.g.  $r_{max} \in [25, 36)$  for  $P \sim 10^5$  (i.e. averaged daily percentage of infected/deceased reaching peaks between 0.025% to 0.036% of the total population), and  $r_{max} \in [3.1 \times 10^3, 7.8 \times 10^3]$  for  $P \sim 10^8$  (peaks between 0.003% and 0.008% of P per day);

- VIII)  $\mathcal{T} \in [6.0, 6.9]$ , very strong events: epidemics characterized by values of  $r_{max} \in [36, 49)$  for small countries with  $P \sim 10^5$ , and  $r_{max} \in [7.8 \times 10^3, 1.7 \times 10^4)$  for large countries with  $P \sim 10^8$ ;
- VIII)  $T \in [7.0, 7.9]$ , violent events: outbreaks featuring e.g. values of  $r_{max} \in [49, 64)$  for  $P \sim 10^5$ , and  $r_{max} \in [1.7 \times 10^4, 3.3 \times 10^4]$  for  $P \sim 10^8$ ;
  - IX)  $T \ge 8.0$ , extreme epidemic events featuring e.g. values of  $r_{max} \ge 64$  for  $P \sim 10^5$ , and  $r_{max} > 3.3 \times 10^4$  for  $P \sim 10^8$ , i.e. outbreaks whose daily percentages of infected/deceased reach peaks respectively larger than 0.06% and 0.03% of the total population.

Similarly to the Richter scale for seismic events, our epidemic magnitude scale  $\mathcal{T}$  characterizes the local (since it depends on the population size) strength of an epidemic in an exponential fashion, so that each jump by class identifies a tenfold increase in daily reported infected/deceased among countries with similar population sizes. When applied to the available data of the SARS-CoV-2 pandemic,  $\mathcal{T}$  yields the repartition of the epidemic events summarized in Tab. I, with respect to which we filled the data points in Fig. 5 with colors ranging from dark blue to dark red for increasing magnitudes. A primary observation is that all the countries of our dataset have experienced epidemic events of magnitude equal or larger than III [66], reflecting the severe and broad impact that the SARS-CoV-2 pandemic has had worldwide. We notice also that the different responses that countries with similar population sizes (e.g.,  $P \sim 10^7$ ) have had to the pandemic spread is nicely captured by  $\mathcal{T}$ , with e.g.

country	T	d	type	country	$\mathcal{T}$	d	type
GRC	2.9	0.7	$IIII^{++}$	CA	5.1	-0.1	$VI^-$
HU	3.0	0.6	$IV^{++}$	NL	5.2	-0.25	$VI^-$
MYS	3.1	0.8	$IV^{++}$	PT	5.2	-0.29	$VI^-$
JP	3.4	0.9	$\mathbb{I}V^{++}$	TU	5.4	-0.17	$VI^-$
AUS	3.7	0.5	$\mathbb{I}V^{++}$	FR	5.6	-0.26	$VI^-$
FIN	3.7	0.2	$IV^+$	GE	5.7	-0.25	$VI^-$
KOR	3.7	0.6	$IV^{++}$	СН	5.8	-0.49	$VI^-$
CHN	3.8	1.1	$\mathbb{I}V^{+++}$	UK	5.9	-0.35	$VI^-$
CZE	3.9	0.2	$\mathbb{I}\mathbb{V}^+$	BE	6.0	-0.52	$VIII^{}$
ROU	3.9	0.3	$IV^+$	ΙE	6.0	-0.58	$VIII^{}$
NO	4.3	-0.1	V	$\operatorname{IT}$	6.0	-0.39	$VIII^-$
IL	4.9	-0.2	$V^-$	US	6.5	-0.45	$VIII^-$
AT	5.1	-0.26	$VI^-$	SP	6.6	-0.62	$ VIII^{} $

TABLE I. Magnitude of SARS-CoV-2 outbreaks. Classification of the SARS-CoV-2 first-wave epidemic events according to their magnitude,  $\mathcal{T}=10^{\kappa/\chi^*}$ , where  $\chi^*\equiv 1-3/\log P$  represents an upper limit to the epidemic "strength" characterizing an outbreak of catastrophic proportions (see Eq. (2) and discussions therein). Nations' intervention efficiency, rated with plus and minus signs, is measured according to the deviation of all countries best linear fit  $d=r_0+\log(P^\beta/r_{max}^{dat})$  from the ordinate  $r_{max}^{dat}$  of each data point (see the main text for more details).

cases like Greece or Hungary both experiencing light outbreaks, and cases like Israel or Switzerland facing instead moderate to strong events (see Tab. I). Very strong pandemic events can be instead recognized by the orange colors in countries like Italy, France or Germany, and even more extreme ones by increasingly red colors describing the cases of the United States (magnitude 6.5) and Spain (magnitude 6.6). Surprisingly, we find that the first-wave epidemic event in Spain features in fact a larger magnitude than the one reported in the United States.

The linear regression analysis in Fig. 5 provides with additional information the classification by magnitude of the SARS-CoV-2 pandemic types. Unlike other catastrophic events, in fact, epidemic outbreaks can be influenced at their early stages by social intervention strategies [30–39], and so do their magnitude scales. While T measures the impact of the pandemic across different countries, the deviation of all countries best linear fit  $d = \log(r_{max}/r_{max}^{dat})$  from the ordinate  $r_{max}^{dat}$  of each data point can be adopted to rate the effectiveness of the intervention strategies adopted. Values of d for the available data and reported in Tab. I, are typically dispersed in the unit interval (dashed green and red lines in Fig. 5) around zero, suggesting the following rating system for the social intervention strategies adopted: +++) for  $d \geq 1$  as reported in countries that, despite their population size, managed to contain the outbreak very efficiently; ++) if  $0.5 \le d \le 0.9$  and +) if  $0 \le d < 0.5$ for countries with efficient to good intervention; —) if  $-0.5 \le d < 0$  and --) if  $-1 \le d < -0.5$  describing instead weak or not prompt responses to the emergent outbreaks. We find (see Fig. 5) that highly populated countries like China or Japan applied successful social intervention protocols which kept low the magnitude of the epidemic events, while other countries like Ireland, Belgium or Spain gained less efficient results, experiencing outbreaks of larger magnitudes.

Outbreak intensity. In the previous section we adopted the epidemic angle  $\theta$  (defined by the inclination of  $r_{max}$ with respect to the I-axes) as an estimator of the "speed" of an epidemic event, with large values of  $\theta$  reflecting highly critical conditions of the country's health system. We have also shown that  $\theta$  is linearly correlated (Fig. 3) to the geometric parameter  $\rho$ , measuring instead the relative width of the epidemic plumes, whose values can be adopted to evaluate the quality of a country's strategies for contact tracing or patient identification. The normalization of the trajectories by  $r_{max}$  shown in Fig. 3a)-f), has highlighted that a further informative quantification of the country's tracking strategies can be obtained by considering the "eccentricity",  $e = \sqrt{1 - \rho^2}$ , of the normalized epidemic plumes. On the one hand, this operation removes all the information about the relative extend of the infected and fatality rates and hence it wipes out the classification of the epidemic events according to the angle  $\theta$ . On the other hand, analyzing the eccentricity of the normalized epidemic plumes yields a more faithful comparison among their forms, clearly isolating

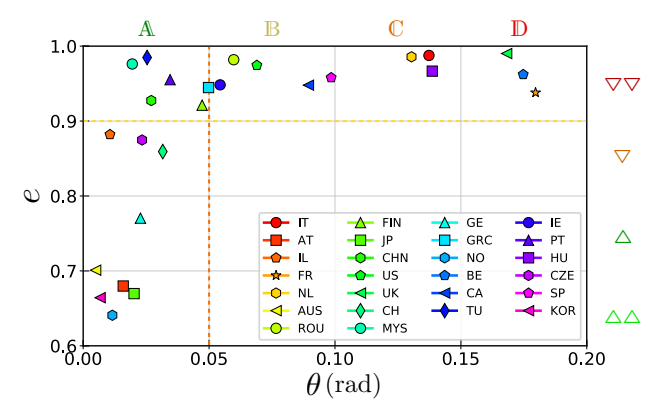


FIG. 6. Intensity scales of typical SARS-CoV-2 epidemic trajectories. (Color online) Hybrid scatter plot describing the distribution of typical epidemic events according to their angle  $\theta$  (raw data) expressed in radians, and eccentricity e (normalized data). Epidemic events with angles larger than the threshold  $\theta^* = 0.05$  (red dashed line) can be taken to describe fast pandemic with increasing speed (categories  $\mathbb{B}$ ,  $\mathbb{C}$ ,  $\mathbb{D}$ ). These categories appear to correspond to epidemic plumes with large eccentricities (class  $\nabla\nabla$ ) and small peakto-peak separation, reflecting late identification of infected patients or selection of diagnostic testing only for critically ill cases. Slow pandemics (i.e. category  $\mathbb{A}$ ), on another hand, disclose a broader spectrum of forms (classes  $\nabla\nabla$ ,  $\nabla$ ,  $\Delta$ ,  $\Delta\Delta$ ) reflecting different strategies of patient identification.

narrow plumes from rounder ones. To make the best out of this trade-off of information, we have created the hybrid scatter-plot  $(\theta,e)$  shown in Fig. 6, where countries' SARS-CoV-2 events are classified according to the angle of their row epidemic data (just as in Fig. 3) and the eccentricity of their normalized plumes. When applied to the available data, this hybrid representation unveils something surprising. We find, in fact, that epidemic angles larger than a threshold value  $\theta^* \equiv 0.05$  always correspond to narrow plumes with normalized eccentricities  $e \in (0.9,1)$ . Instead, plumes with  $\theta < \theta^*$  can correspond to a broader spectrum of forms, from the round ones reported in Japan, Austria or Germany, to more narrow types like those of Canada, Portugal or Turkey.

To explain this surprising pattern, let us notice that the main factor decreasing the eccentricity of a normalized epidemic plume is an increasing time lag between the infected and fatality rate peaks which, in its turn, suggests that the data of reported infected and deceased are less likely correlated. The eccentricity can then be adopted for comparing the countries' strategies for patient identification, with small values of e characterizing efficient tracking protocols, and large values of e describing instead situations where the majority of the fatalities were infected patients tested positive only after arriving at the hospitals in critical conditions. This is probably best represented in Fig. 6 by cases like the United Kingdom ( $e \simeq 0.990$ ), Italy ( $e \simeq 0.987$ ) or the Netherlands  $(e \simeq 0.985)$  which all experienced violent outbreaks with identification only of critically ill patients [67] and highly critical conditions ( $\theta > \theta^*$ ) of their medical system [68].

Fig. 6 suggests therefore the following data-driven clas-

sification by *intensity*, i.e. based on the damage produced on the population, of the SARS-CoV-2 events:

- A)  $\theta < \theta^*$ , slow pandemics: low values (1.4% in Australia to 6.1% in Greece [62]) of the largest case-fatality rate, well functioning health system;
- B)  $\theta^* \leq \theta < 0.1$ , moderately-fast pandemics: higher (6.8% in Ireland to 12.2% in Spain) case-fatality rates, mild disruption of the medical system;
- $\mathbb{C}$ )  $0.1 \leq \theta < 0.15$ , fast pandemics: severe disruption of the health system, possibility of strategic triage, high (12% in the Netherlands to 14.1% in Hungary) largest case-fatality rate;
- D)  $\theta \geq 0.15$ , very fast pandemics: very high (15.9% in the United Kingdom to 19% in France) largest case-fatality rate, medical crisis, strategic triage.

Similarly to the magnitude,  $\mathcal{T}$ , the epidemic intensity scale can be accompanied by a rating system quantifying in this case the efficiency of patient identification and contact tracing strategies, suitably defined as follows:  $\triangle \triangle$ ) plumes with eccentricity  $e \leq 0.7$ , featured by countries that performed extensive testing and rapid patient identification, resulting in less correlated data series for infected and deceased rates as reflected by large peak-to-peak time lags;  $\triangle$ ) plumes with eccentricities  $0.7 < e \le 0.8$ , describing good patient identification;  $\nabla$ ) plumes with eccentricity  $0.8 < e \le 0.9$ , describing mildly efficient patient identification;  $\nabla\nabla$  plumes having eccentricity e > 0.9 and strong peak-to-peak proximity, reflecting weak or not-efficient identification strategies. This classification reflects, in a quantitative fashion, a simple vet essential fact regarding the fight against the SARS-CoV-2 virus: rapid patient identification leads to functional health system and low case-fatality rates (category  $\mathbb{A}^{\triangle\triangle}$ ), whereas less and less efficient strategies lead more often to fast pandemics (categories B-D) depending on the country's hospital capacities.

4. Temporal evolution of the epidemic angle. The introduction of the epidemic magnitude (Fig. 5 and Tab. I) and intensity (Fig. (6)) enabled a preliminary vet informative classification of the SARS-CoV-2 pandemic events, highlighting the main ingredients underlying their epidemiometric fingerprints. An important byproduct of this result lies in the possibility of designing alarm protocols and other precautionary measures to dampen the societal effects of a pandemic event [1, 2]. In fact, understanding the magnitude and intensity of the SARS-CoV-2 epidemic events could help policy-makers to make informative decisions not only for investing resources to strengthen a country' health system, but it can enhance the public awareness with the design of alarms platforms aiming at facilitating contact tracing or promoting responsible actions of social-distancing.

Unlike other catastrophic events, in fact, the magnitude and intensity of a pandemic lie entirely in the hands

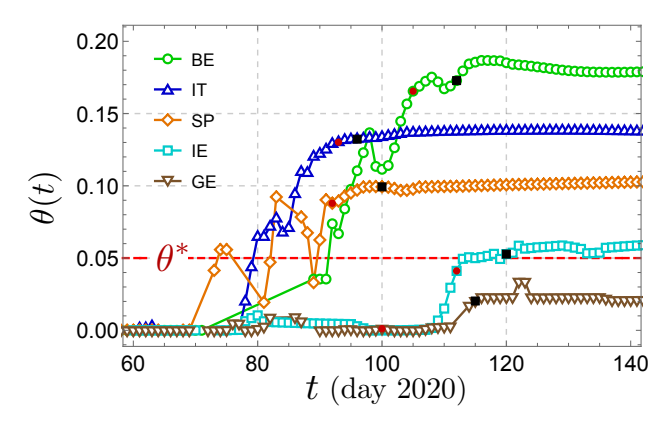


FIG. 7. Evolution of the epidemic angle. (Color online) Temporal evolution of the epidemic angle for different countries' plumes, obtained by best fitting the data series (smoothened by a 15-day moving average) with a daily update of their epidemic state. Countries experiencing fast epidemic events of category  $\mathbb{C}^{--}$  or higher cross the threshold angle  $\theta^*$  (red dashed line) way before reaching their infected peaks (red filled markers) and fatality peaks (black filled markers). Slow epidemics, like in Germany, keep instead their epidemic angle below  $\theta^*$  already when reaching the infected peak.

of the countries' governments, their preparedness to absorb the impact of a rapidly emerging outbreak, and the awareness of societies to its potential damage. In this light, quick actions at the early stages of an epidemic outbreak in tracking the infected [48] or more efficient social intervention protocols [36, 38] can help curbing down dramatically [30, 69] its devastating effects. This is why an early estimation of the outbreak scales could significantly help designing epidemic alerts for enhancing the public and governmental awareness and help fighting against the virus spreading. In this context, understanding how the SARS-CoV-2 epidemic scales evolve in time could provide significant information for future design of early warning systems [20] and risk alerts [19].

Motivated by this idea, we have analyzed in Fig. 7 the temporal evolution of the epidemic angle  $\theta$  for a few representative countries of Fig. 6. The results in Fig. 7 show that countries having experienced fast pandemics of category  $\mathbb{C}^{\triangledown\triangledown}$  or higher such as Italy, Spain or Belgium, all crossed the critical angle  $\theta^*$  long before reaching their infected peaks (red filled circles), reflecting a slow responsiveness [70] to the rapidly emerging outbreak. On the contrary, countries like Germany (or Austria and Switzerland, not shown in Fig. 7 to simplify the exposition) succeeded in keeping  $\theta$  below  $\theta^*$  already when they reached their infected rate peaks, suggesting efficient patient identification and well functioning medical systems. Advanced knowledge of the epidemic intensity could have helped countries like Italy or Spain in adjusting more rapidly their policies of contact tracing and identification of seriously ill patients, offering more options of intervention to fight the epidemic crisis.

5. Low-dimensional parametrization. Our geometric analysis additionally hints at an integrated, low-dimensional parametrization for modeling the evolution

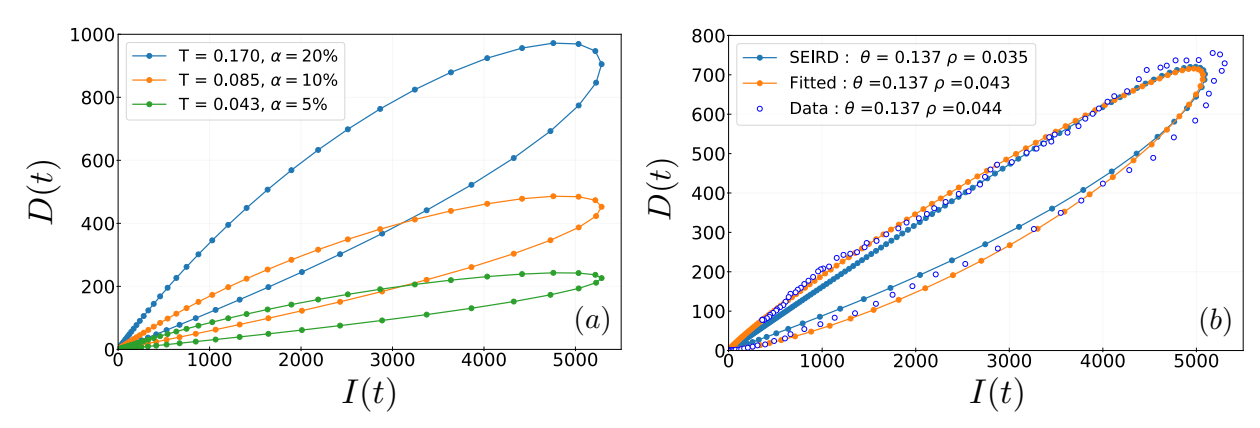


FIG. 8. **SEIRD trajectories and low-dimensional parametrization.** (Color online) **a)** Representation in the (I, D) plane of typical (Fig. ??) epidemic trajectories obtained by solving Eqs. 3 with fixed parameters  $(\gamma, \sigma, \mu, R_{0,i}, R_{0,f}, \kappa, \tau) = (1/3, 1/5, 1/3, 8, 0, 0, 0)$  and decreasing fatality rates  $\alpha = (1/5, 1/10, 1/20)$  (presented as percentages in the legend). This choice of parameters describes an epidemic similar to SARS-CoV-2 but with constant reproduction rate  $R_0 = 4$ , where individuals incubate the virus for an average period of 5 days, gets infected at rate  $\beta \simeq 1.33$ , and recover/die in an average period of 3 days. **b)** Demonstration of the SEIRD trajectory obtained by manual searching for epidemiological parameters matching the data-driven geometric constraints. For the Italian outbreak (open markers), this low-dimensional analysis leads to an SEIRD trajectory (blue curve) characterized by the parameters  $(\gamma, \sigma, \alpha, \mu, R_{0,i}, R_{0,f}, \kappa, \tau) = (1/3, 1/5, 1/7, 1/2.95, 3.89, 0.98, 0.24, 44)$  whose features are qualitatively similar to those characterizing the best-fitting pseudo-ellipses (orange curve).

of real-world epidemic trajectories. In fact, the geometric parametrization of the epidemic plumes allows (at least, on the coarse-grained level of the national trends) to curtail with a few parameters the essential information ruling the epidemic spreading [28, 51], out of a variety of epidemiological factors, from e.g. different gender-based transmission factors [71–73], to mobility patterns [74, 75] and social mixing [38, 76], to cities' pollution [19], different quarantine [77] or testing strategies [78] and many others. Even when adopting a well-mixed approximation among different compartments, developing a predictive framework embracing such a variety of factors easily results into mathematical or computational tour deforces [27, 55, 56] whose complexity quickly grows with the number of realistic features included.

From another viewpoint, modern epidemic models based either on detailed descriptions of the population's compartments [30, 56, 79] or merging simplified versions of the latter with tools of bayesian inference [27] and neural networks [80], typically yield predictions of a country's epidemic trend after fitting either its data for the infected rates or the ones fo the fatality rates. This separated approach leads to best-fitting epidemiological factors that, when adopted to describe the behaviors of other compartments which have not been fitted to the data, lead to results far from the real-world trends.

Our geometric approach offers a viable solution to circumvent both these limitations by best-fitting the synthetic epidemic plumes directly to the data-driven ones, enabling in this way an *integrated* and *low-dimensional* estimation of the epidemiological parameters best describing the outbreak evolution.

As a demonstrative example, let us consider an SEIRD epidemic model [81, 82] to describe the SARS-CoV-2 dynamics. For completeness, let us recall that the SEIRD

model suitably characterizes the spreading of a viral agent featuring a latent (sometimes also referred to as cryptic [83]) phase where susceptible individuals (S) become exposed (E), i.e. they acquire the infection but are not yet infectious. After a characteristic incubation period  $1/\sigma$  days (with  $\sigma \in (0,1]$ ), exposed individuals become infectious (I) and start spreading the disease at a speed,  $\lambda$ , controlling the average number of people an infected person infects per day. Infected individuals spread the disease during an average period of  $1/\gamma$  days (with  $\gamma \in (0,1]$ ), after which they either recover (R) or die (D). Let  $1/\mu$  (with  $\mu \in (0,1]$ ) be the characteristic period of days during which an infected individual becomes critically ill and eventually dies, and  $\alpha \in [0,1]$  the fatality rate characterizing instead the probability of going from infected to death (i.e.,  $\alpha$ ), and from infected to recovered (i.e.,  $1-\alpha$ ). The parameters  $\lambda, \sigma, \gamma, \mu, \alpha$  define respectively the infectious, incubation, recovery, mortality and fatality rates of the SEIRD model; to simplify the analysis, let us assume that once recovered, individuals gain immunity. The above epidemic process is summarized in the system of differential equations:

$$S' = -\lambda sI, \quad E' = \lambda sI - \sigma E$$

$$I' = \sigma E - (1 - \alpha)\gamma I - \alpha \mu I,$$

$$R' = (1 - \alpha)\gamma I, \quad D' = \alpha \mu I,$$
(3)

where  $s \equiv S/N$  is the density of susceptible individuals and N the population size. As a last ingredient, let us include in Eq. 3 the additional information of a time dependent infectious rate  $\lambda(t)$ , identifying the introduction of social distancing measures and quarantine strategies. These, in fact, aim at lowering the basic reproduction number  $R_0 = \lambda/\gamma$  of the virus from a certain initial

value  $R_{0,i} > 1$  to a final one  $R_{0,f} < 1$ . To model this decay, whose speed will depend on the efficiency of the lockdown strategy applied by a country, let us adopt a logistic function of the form

$$R_0(t) = \frac{R_{0,i} - R_{0,f}}{1 + e^{\kappa(t - \tau)}} + R_{0,f}, \tag{4}$$

where  $\tau$ ,  $\kappa \geq 0$  are two "intervention" parameters ruling respectively the time of the inflection point in the profile of  $R_0(t)$  (i.e. the day of the country's main lockdown) and the decay rate of the reproduction number as a result of the lockdown efficacy. In particular, values of  $\kappa \sim \mathcal{O}(1)$  result into a fast decay of  $R_0(t)$  (signaling a rapid and efficient intervention), while  $\kappa \sim 10^{-1}$  or smaller results into a very slow convergence towards  $R_{0,f}$ .

Already at this simplistic level, the epidemiological  $(\lambda, \sigma, \gamma, \mu, \alpha, R_{0,i}, R_{0,f})$  and intervention  $(\tau, \kappa)$  parameters aiming at representing the data-driven epidemic plumes, identify an 8-dimensional phase space for the dynamical system in Eq. (3). Thanks to our geometric parametrization, it proves possible to find the functional dependences relating this variety of parameters to the three geometric factors  $(r_{max}, \theta, e)$ , whose relations identify a series of data-driven parametric constraints to reduce the degrees of freedom of the problem. Finding the exact dependence between the epidemiological variables and the geometric factors is beyond the scope of the present work and will be discussed elsewhere. Nevertheless, it is immediate to verify that e.g. an increase of the case-fatality rate  $\alpha$  leads to an increase of the epidemic angle (Fig. 8a)—i.e. larger epidemic intensities while increasing the infection rate  $\lambda$  yields larger values of  $r_{max}$ —i.e. larger epidemic magnitudes—supporting our heuristic arguments in Sec. 3.

Fig. 8b demonstrates this integrated, low-dimensional approach applied to the Italian epidemic data. We have performed a manual search of the epidemiological parameters best fitting the data-driven values  $\theta_{IT} \simeq 0.137$  and  $\rho_{IT} \simeq 0.44$ , selecting a suitable sub-manifold of the phase space featuring trajectories geometrically congruent to the data-driven one. Even if they do not best-fit the data-driven plumes (empty markers and blue curve in Fig. 8b), the set of parameters we identified generates a SEIRD plume nicely matching the epidemic data. In particular, we find that a relatively large initial reproduction number  $R_{0,i}^{IT} \simeq 3.9$  (in qualitative agreement to the more precise ones obtained by best fitting regional data [84]) and a low lockdown efficiency parameter  $\kappa_{IT} \simeq 0.24$ , reflecting the slow decay already observed in Fig. (1) and therein quantified by a high infected rate skewness. The low-dimensional analysis further discloses another realistic ingredient characterizing the Italian pandemic type, i.e. the high case-fatality rate  $\sigma_{IT} \simeq 14.2\%$  reflecting the strong intensity of the Italian outbreak and the critical conditions reached by its health care system. Further developing these geometric-based concepts could lead to the identification of additional parametric constraints further reducing the degrees of freedom of epidemic models, pos-

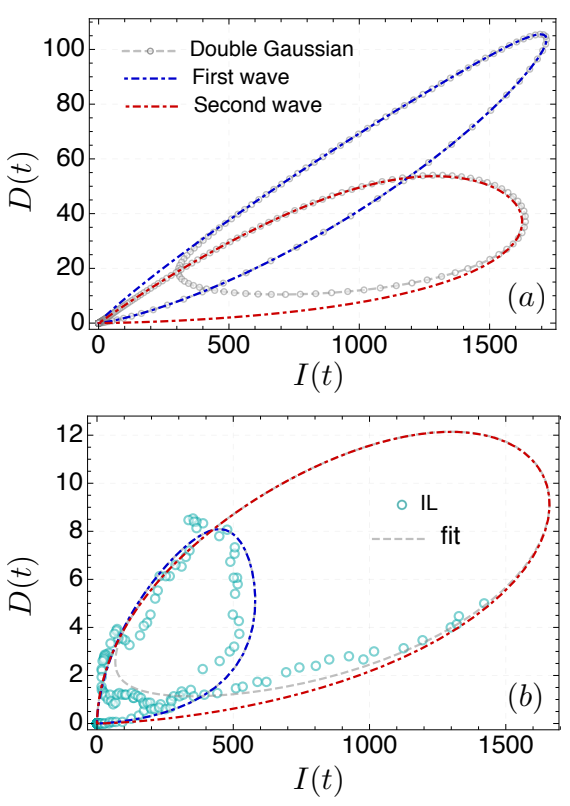


FIG. 9. Second-wave analysis. a) Synthetic data (gray circles) generated by considering for both the infected and the fatality rates bimodal skewed Gaussians with well resolved first- and second-wave peaks. The two trajectories, describing respectively the first (blue dot-dashed curve) and second (red dot-dashed curve) waves, are analyzed by separating the corresponding fitting plumes. Both the epidemic events have same magnitude but different epidemic angles, with the first wave of category B and the second one of category A. b) Epidemic data describing the evolution of the outbreak in Israel (darker cyan circles) and its fitted double-plume trajectory (gray dashed curve). By separating each fitting curve as in a) we identify the first epidemic wave (blue, dot-dashed curve) of magnitude  $T_1 \simeq 4.9$  and category  $A^-$ , and the ongoing second wave (red, dot-dashed curve). As of July 20 2020, the second-wave event in Israel has epidemic angle  $\theta_{IL} \simeq 0.005$ (i.e. category A), and magnitude  $T_2 \simeq 6.6$  (i.e. class VII).

sibly boosting their forecasting power. Considering additional information coming e.g. from the different curvilinear velocities of the right and left lobes of the epidemic plumes, the local curvature of their traces may yield unfamiliar perspectives in achieving this task.

6. Future directions. Our study is only a preliminary step in the design of metric systems for epidemic events. We expect that the results will inspire the development of more refined epidemiometric frameworks for rating the magnitude and the impact of present and future epidemics, helping governments and other decision-makers to strengthen their policies of containment and better respond to such extreme events. In this perspective, we highlight in what follows a few important directions of future research in which respect we believe that our geometric approach could be further developed.

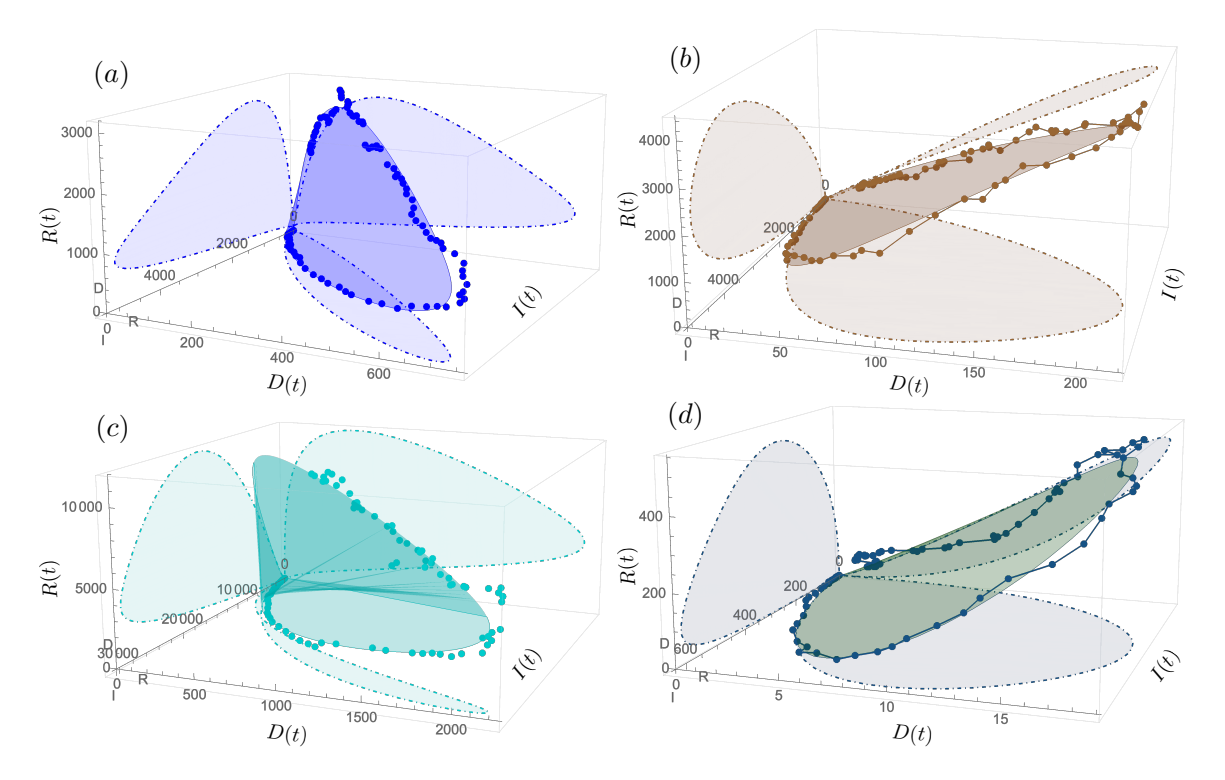


FIG. 10. **SARS-CoV-2 epidemic surfaces.** Evolution in the (I, D, R) space of the data (markers) describing the epidemic state for a selection of countries: **a**) Italy, **b**) Germany, **c**) United states and **d**) Austria. Data have been selected to identify the first-wave event for each country, where a second one was observed. Each trajectory traces a surface (shadowed areas) whose projections on the (I, D), (I, R) and (R, D) planes are further shown. While Italy's surface unfolds in the space almost perpendicular to the (I, D) plane (where it traces the narrow trajectory discussed in Fig. 8b), Germany's surface unfolds nearly parallel to the (I, D) plane, tracing instead a rounder pseudo-ellipses (i.e. larger normalized eccentricity). Behaviors respectively similar to **a**) Italy and **b**) Germany are observed in **c**) the United States, as well as in Spain or France (with the last two not shown in the above to ease the exposition) and in **d**) Austria, as well as Switzerland or Australia (not shown).

i) Beyond first-waves. Our analysis focused on typical (i.e. counter-clockwise evolving) epidemic trajectories describing the first-wave events of the SARS-CoV-2 pandemic in a selection of countries. As of July 20 2020, some nations included in our analysis have entered secondary epidemic waves whose magnitude appears already to be larger than the classification in Tab. I; this is the case of e.g. the United States, Iran, Israel or Serbia. Extending the geometric method to secondary waves is possible as long as the first and the second-wave peaks of the infected and deceased rates are sufficiently resolved over time (Fig. 9a). In this case, fitting the data by multiple (skewed) Gaussians allows to trace a new epidemic trajectory in the (I, D) plane whose evolution may cross itself and disclose geometric features significantly different from those of the first wave. By isolating the fitting functions describing each lobe (Fig. 9a), it is possible to perform an analysis perfectly analogous to the one described above for the case of first-waves, identifying the epidemic angle  $\theta$ , largest extend  $r_{max}$  and eccentricity eof the second-wave trajectory. As most of the nations that entered the second wave have not yet reached their new infected peak, we cannot yet draw conclusive evaluation about the magnitude and intensity of their new

epidemic events, but we track the evolution of the geometric parameters characterizing their new trajectories as suggested in Sec. 5 (see Fig. 7). In Fig. 9b we have presented the epidemic trajectories describing the state of Israel. A preliminary evaluation shows that while the new wave has already a magnitude  $\mathcal{T}_2 \simeq 6.6$ , i.e. a very strong epidemic event comparable to the first-wave event of Spain or US (see Sec. 3), its epidemic angle is still relatively low ( $\theta_{IL} < 0.005$ ) with respect to the threshold value  $\theta^* = 0.05$  of the onset of a fast pandemic (Fig. 6). Comparing the magnitude and intensity of different epidemic events in the same country could help understanding how different countries prepared themselves to absorb and dampen the impact of a new wave of epidemic events.

ii) Including daily testing data. An important direction of future research for improving the epidemic measures defined in the above concerns the inclusion of the information related to the number of daily testing performed by each country. Depending on their resources, in fact, different countries applied different strategies of testing or contact tracing in their fight [85] against the spread of SARS-CoV-2. Germany or Russia, for example, have been performing a tremendous amount of tests since the early stages of the pandemics and over a very broad [86]

fraction of the population, including both symptomatic and asymptomatic patients. Countries like Italy [67] or Spain [87] had instead to prioritize their diagnostic capacities to test patients with more severe clinical symptoms and in need of hospitalization. Including this relevant bit of information in the analysis above, e.g. by normalizing the number of new daily infected by the corresponding number of daily new tests, would possibly result into an even more meaningful comparison of the countries epidemic magnitude than the one in Tab. I and, likewise, of the classification by intensity depicted in Fig. 6.

iii) Zooming-in: local characterization of countries pandemic types. Our results have focused on analyzing the epidemic trends reported at national levels, offering a country-to-country comparison of their SARS-CoV-2 pandemic types. The epidemiometric system of epidemic events proposed however, can be equivalently adopted to analyze more local datasets of each country, offering a magnifying lens to determine the magnitude and the intensity of the epidemic events observed within states, regions or even on the smaller scales of provinces and towns. In the case of Italy, for example, regions such as Lombardia, Emilia-Romagna, Piemonte and Veneto have suffered more severe epidemic events than the rest of the country [19], and a similar situation has been reported in United States for the states of New York, California and (more recently) of Florida [88]. An efficient intervention at the national level could find its crucial ingredients in a rapid intervention on the level of its states. regions or provinces. Combined with forecasting tools and prior epidemic risk assessments, our epidemiometric framework could provide the design of local epidemic alerts to enhance the awareness of governments and inhabitants already at local levels, helping to counter the spreading of highly infectious viruses like SARS-CoV-2.

iv) Geometry of the epidemic surfaces. As a conclusive remark, let us notice that in our developed geometric analysis, we have focused only on the projections of the epidemic trajectories in the (I, D) plane. However, other compartments (e.g. recovered, critical patients, active cases, etc) can be included in the analysis, resulting in a multi-dimensional representation of the epidemic state of each country. For instance, the addition of the compartment of daily recovered (R) yields the emergence of new information to further refine the classification of the pandemic fingerprints reported in different nations. Fig. 10) contains a few examples of "epidemic surfaces" in the (I, D, R) 3D-space observed in a selection of countries. In particular, the cases of Italy (Fig. 10a) and Germany (Fig. 10b) clearly exhibit striking differences in their dynamic evolution: Italy's epidemic surface features a narrow cross-section in its projection on the (I, D)plane and a broad trajectory in the (R, D) plane, as opposed to the epidemic surface characterizing Germany's outbreak. The two surfaces, in fact, appear to be roughly orthogonal with each other, a clear indication that in Italy the increase of infected yielded a rapid and simultaneous increase of deceased. Similar behaviors can be

found in cases belonging to the same magnitude and intensity. For example, Austria (Fig. 10d) as well as Norway or Switzerland shares similar patterns to those observed in Germany, while countries like USA, France or Spain feature inclinations of their epidemic surfaces resembling the one observed in Italy.

The identification of the patterns shared by the outbreaks of different countries would have otherwise been impossible if we had to limit our view to the classical time evolution of the epidemic compartments as in Fig. 1. Exploring epidemic dynamics from this novel, geometric-based perspective could unveil new "hidden" features characterizing their evolution and foster new methods for their statistical analysis and mathematical modeling. We expect that our geometric framework and results will inspire alternative approaches to the study of epidemic evolution, possibly leading to longer-termed forecasting techniques or to more refined epidemiometric systems for the design of epidemic alerts and early warning systems.

7. Discussion. We have presented a geometric framework to analyze and systematically classify the trajectories of the SARS-CoV-2 pandemic across different countries in the (I, D) plane via three geometric parameters  $(r_{max}, \theta, e)$ . Our geometric measures enables the design of a preliminary epidemiometric system to quantify the magnitude of a country's outbreak and its intensity, resembling respectively the Richter and the Mercalli measures for seismic events, and further adding information about the efficacy of lockdown strategies and of patient identification. The epidemic scale measures we defined help identifying a spectrum of SARS-CoV-2 pandemic types, ranging from weak epidemic events with slow speed, like those reported in Japan, Australia or South Korea (magnitude  $T \simeq 3.4$ , class ++, category  $\mathbb{A}^{++}$ ), to very extreme events with intense damage inflicted on the population, like the cases of United Kingdom (magnitude  $T \simeq 5.9$ , class --, category  $\mathbb{D}^{--}$ ) or Italy (magnitude  $\mathcal{T} \simeq 6.0$ , class –, category  $\mathbb{C}^-$ ).

However, unlike other catastrophic events, the magnitude and intensity of an epidemic event entirely depends on the responsiveness of the countries' government and the capacity of their medical systems, jointly with the awareness of their population to their potential damage. In this respect, early estimation of the epidemic scales (e.g. by merging them with forecasting models) could significantly contribute to the design of warning systems [19, 20] or protocols for virus alerts to enhance the public and governmental responsiveness. We showed that, in cases like Italy or Spain (Fig. 7), the epidemic angle  $\theta$  has crossed the threshold  $\theta^* = 0.05 \text{rad}$  from slow to fast pandemics way before reaching the infected and fatality peaks, reflecting a slow responsiveness to the rapidly emerging crisis. From the mathematical perspective, our geometric method further raises relevant insights to improve current epidemic models. The geometric characterization of the epidemic plumes in the (I, D) plane, discloses an integrated and low-dimensional approach to modeling the epidemic trends by imposing

geometric constraints relating the data-driven parameters  $(r_{max}, \theta, e)$  to the epidemiological factors entering the epidemic models adopted. This allows to lower the number of independent parameters, identifying a suitable sub-manifold of the high dimensional phase space where plumes congruent to the data-driven ones can be found. We have demonstrated this approach by manually searching, in an SEIRD model with a time-dependent reproductive number, the best choices of the epidemiological and intervention parameters satisfying the data-driven geometric constraints for the Italian trends, obtaining a realistic description of the reported behaviors.

We foresee that the merging of our data-driven, low-

dimensional approach with more advanced mathematical or computational methods [27, 80], could lead to predictions of the epidemiometric fingerprints of real-world epidemics with ever-increasing accuracy, possibly disclosing new directions to the identification of optimal priors for more efficient and longer-termed epidemic forecasting.

Acknowledgements S.H. thanks the Israel Science Foundation, ONR, the BIU Center for Research in Applied Cryptography and Cyber Security, NSF-BSF Grant no. 2019740, and DTRA Grant no. HDTRA-1-19-1-0016 for financial support. I.B. thanks A. Collini and M. Hidalgo Soria for valuable discussions.

- Havidán Rodríguez, Enrico Louis Quarantelli, Russell Rowe Dynes, William A Andersson, Patrick A Kennedy, and Everett Ressler. *Handbook of disaster re*search, volume 643. Springer, 2007.
- [2] Piers Blaikie, Terry Cannon, Ian Davis, and Ben Wisner. At risk: natural hazards, people's vulnerability and disasters. Routledge, 2014.
- [3] Henry Farrell and Abraham Newman. Will the coronavirus end globalization as we know it? *Foreign Affairs*, 16, 2020.
- [4] Aamer Raza. Coronavirus and the future of globalization. Review of Human Rights, 6(1):xxxii-xxxvi, 2020.
- [5] Charles F Richter. An instrumental earthquake magnitude scale. Bulletin of the seismological society of America, 25(1):1–32, 1935.
- [6] Giuseppe Mercalli. Sulle modificazioni proposte alla scala sismica De Rossi-Forel, volume 8. Società tipografica modenese, 1902.
- [7] Hiroo Kanamori, Egill Hauksson, and Thomas Heaton. Real-time seismology and earthquake hazard mitigation. *Nature*, 390(6659):461–464, 1997.
- [8] JM Espinosa Aranda, A Jimenez, G Ibarrola, F Alcantar, A Aguilar, M Inostroza, and S Maldonado. Mexico city seismic alert system. Seismological Research Letters, 66(6):42–53, 1995.
- [9] Hiroo Kanamori. Real-time seismology and earthquake damage mitigation. Annu. Rev. Earth Planet. Sci., 33:195–214, 2005.
- [10] Shigeki Horiuchi, Hiroaki Negishi, Kana Abe, Aya Kamimura, and Yukio Fujinawa. An automatic processing system for broadcasting earthquake alarms. *Bulletin* of the Seismological Society of America, 95(2):708–718, 2005.
- [11] Robert K Reitherman. Earthquakes and engineers: an international history. American Society of Civil Engineers, 2012.
- [12] Younes Achaoui, Bogdan Ungureanu, Stefan Enoch, Stéphane Brûlé, and Sébastien Guenneau. Seismic waves damping with arrays of inertial resonators. *Extreme Mechanics Letters*, 8:30–37, 2016.
- [13] Tetsuya Theodore Fujita. Proposed characterization of tornadoes and hurricanes by area and intensity. 1971.
- [14] Herbert S Saffir. Hurricane wind and storm surge. The Military Engineer, 65(423):4–5, 1973.
- [15] Robert H Simpson and H Saffir. The hurricane disaster

- potential scale. Weatherwise, 27(8):169, 1974.
- [16] Jerry Keith Barber. Tornado warning system, September 25 2001. US Patent 6,295,001.
- [17] John H Sorensen. Hazard warning systems: Review of 20 years of progress. Natural hazards review, 1(2):119–125, 2000.
- [18] Burrell E Montz, Graham A Tobin, and Ronald R Hagelman. Natural hazards: explanation and integration. Guilford Publications, 2017.
- [19] A Pluchino, G Inturri, A Rapisarda, AE Biondo, R Le Moli, C Zappala, N Giuffrida, G Russo, and V Latora. A novel methodology for epidemic risk assessment: the case of covid-19 outbreak in italy. arXiv preprint arXiv:2004.02739, 2020.
- [20] Nicole E Kogan, Leonardo Clemente, Parker Liautaud, Justin Kaashoek, Nicholas B Link, Andre T Nguyen, Fred S Lu, Peter Huybers, Bernd Resch, Clemens Havas, et al. An early warning approach to monitor covid-19 activity with multiple digital traces in near real-time. arXiv preprint arXiv:2007.00756, 2020.
- [21] Matjaž Perc, Nina Gorišek Miksić, Mitja Slavinec, and Andraž Stožer. Forecasting covid-19. Frontiers in Physics, 8:127, 2020.
- [22] Vinko Zlatić, Irena Barjašić, Andrea Kadović, Hrvoje Štefančić, and Andrea Gabrielli. Bi-stability of sudr+ k model of epidemics and test kits applied to covid-19. arXiv preprint arXiv:2003.08479, 2020.
- [23] Fotios Petropoulos and Spyros Makridakis. Forecasting the novel coronavirus covid-19. PloS one, 15(3):e0231236, 2020.
- [24] Duccio Fanelli and Francesco Piazza. Analysis and forecast of covid-19 spreading in china, italy and france. Chaos, Solitons & Fractals, 134:109761, 2020.
- [25] Didier Sornette, Euan Mearns, Michael Schatz, Ke Wu, et al. Interpreting, analysing and modelling covid-19 mortality data. Swiss Finance Institute Research Paper, (20-27), 2020.
- [26] Simon Pollett, Michael Johansson, Matthew Biggerstaff, Lindsay C Morton, Sara L Bazaco, David M Brett Major, Anna M Stewart-Ibarra, Julie A Pavlin, Suzanne Mate, Rachel Sippy, et al. Identification and evaluation of epidemic prediction and forecasting reporting guidelines: A systematic review and a call for action. *Epidemics*, page 100400, 2020.
- [27] Jonas Dehning et al. Inferring change points in the spread

- of covid-19 reveals the effectiveness of interventions. Science, 2020.
- [28] Alessandro Vespignani et al. Modelling covid-19. *Nature Reviews Physics*, pages 1–3, 2020.
- [29] PHP Cintra, MF Citeli, and FN Fontinele. Mathematical models for describing and predicting the covid-19 pandemic crisis. arXiv preprint arXiv:2006.02507, 2020.
- [30] Benjamin F Maier and Dirk Brockmann. Effective containment explains subexponential growth in recent confirmed covid-19 cases in china. *Science*, 368(6492):742–746, 2020.
- [31] Neil M Ferguson, Derek AT Cummings, Christophe Fraser, James C Cajka, Philip C Cooley, and Donald S Burke. Strategies for mitigating an influenza pandemic. Nature, 442(7101):448–452, 2006.
- [32] Timothy C Germann, Kai Kadau, Ira M Longini, and Catherine A Macken. Mitigation strategies for pandemic influenza in the united states. *Proceedings of the National Academy of Sciences*, 103(15):5935–5940, 2006.
- [33] Christopher Adolph, Kenya Amano, Bree Bang-Jensen, Nancy Fullman, and John Wilkerson. Pandemic politics: Timing state-level social distancing responses to covid-19. medRxiv, 2020.
- [34] Stephen S Morse, Richard L Garwin, and Paula J Olsiewski. Next flu pandemic: what to do until the vaccine arrives? 2006.
- [35] Aditya Mate, Jackson A Killian, Bryan Wilder, Marie Charpignon, Ananya Awasthi, Milind Tambe, and Maimuna S Majumder. Evaluating covid-19 lockdown policies for india: A preliminary modeling assessment for individual states. Available at SSRN 3575207, 2020.
- [36] Dror Meidan, Reuven Cohen, Simcha Haber, and Baruch Barzel. An alternating lock-down strategy for sustainable mitigation of covid-19. arXiv preprint arXiv:2004.01453, 2020.
- [37] Omer Karin, Yinon M Bar-On, Tomer Milo, Itay Katzir, Avi Mayo, Yael Korem, Boaz Dudovich, Eran Yashiv, Amos J Zehavi, Nadav Davidovich, et al. Adaptive cyclic exit strategies from lockdown to suppress covid-19 and allow economic activity. medRxiv, 2020.
- [38] Per Block, Marion Hoffman, Isabel J Raabe, Jennifer Beam Dowd, Charles Rahal, Ridhi Kashyap, and Melinda C Mills. Social network-based distancing strategies to flatten the covid-19 curve in a post-lockdown world. Nature Human Behaviour, pages 1–9, 2020.
- [39] Alberto Aleta and Yamir Moreno. Evaluation of the potential incidence of covid-19 and effectiveness of containment measures in spain: a data-driven approach. BMC medicine, 18:1–12, 2020.
- [40] Titan M Alon, Matthias Doepke, Jane Olmstead-Rumsey, and Michele Tertilt. The impact of covid-19 on gender equality. Technical report, National Bureau of Economic Research, 2020.
- [41] Clare Wenham, Julia Smith, and Rosemary Morgan. Covid-19: the gendered impacts of the outbreak. The Lancet, 395(10227):846–848, 2020.
- [42] Joshua R Goldstein and Ronald D Lee. Demographic perspectives on mortality of covid-19 and other epidemics. Technical report, National Bureau of Economic Research, 2020
- [43] Bnaya Gross et al. Spatio-temporal propagation of covid-19 pandemics. medRxiv, 2020.
- [44] Matteo Chinazzi et al. The effect of travel restrictions on the spread of the 2019 novel coronavirus (covid-19)

- outbreak. Science, 368(6489):395-400, 2020.
- [45] Moritz UG Kraemer et al. The effect of human mobility and control measures on the covid-19 epidemic in china. *Science*, 368(6490):493–497, 2020.
- [46] Alberto Aleta, Qitong Hu, Jiachen Ye, Peng Ji, and Yamir Moreno. A data-driven assessment of early travel restrictions related to the spreading of the novel covid-19 within mainland china. *Chaos, Solitons & Fractals*, page 110068, 2020.
- [47] Frank Schlosser, Benjamin F Maier, David Hinrichs, Adrian Zachariae, and Dirk Brockmann. Covid-19 lockdown induces structural changes in mobility networksimplication for mitigating disease dynamics. arXiv preprint arXiv:2007.01583, 2020.
- [48] Ben Moscovitch, John D Halamka, and Shaun Grannis. Better patient identification could help fight the coronavirus. *npj Digital Medicine*, 3(1):1–2, 2020.
- [49] Eran Segal, Feng Zhang, Xihong Lin, Gary King, Ophir Shalem, Smadar Shilo, William E Allen, Faisal Alquaddoomi, Han Altae-Tran, Simon Anders, et al. Building an international consortium for tracking coronavirus health status. *Nature Medicine*, pages 1–4, 2020.
- [50] Giacomo Grasselli, Antonio Pesenti, and Maurizio Cecconi. Critical care utilization for the covid-19 outbreak in lombardy, italy: early experience and forecast during an emergency response. *Jama*, 323(16):1545–1546, 2020.
- [51] Weston C Roda, Marie B Varughese, Donglin Han, and Michael Y Li. Why is it difficult to accurately predict the covid-19 epidemic? *Infectious Disease Modelling*, 2020.
- [52] Henry Loeffler-Wirth, Maria Schmidt, and Hans Binder. Covid-19 trajectories: Monitoring pandemic in the world-wide context. medRxiv, 2020.
- [53] Katherine Ognyanova, Roy H Perlis, Matthew Baum, David Lazer, James Druckman, Mauricio Santillana, and John Della Volpe. The state of the nation: A 50-state covid-19 survey report# 4, 2020.
- [54] Lucas Squillante, Isys F Mello, Antonio C Seridonio, and Mariano de Souza. Attacking the covid-19 with the isingmodel and the fermi-dirac distribution function. arXiv preprint arXiv:2003.11860, 2020.
- [55] Mario Castro, Saúl Ares, José A Cuesta, and Susanna Manrubia. Predictability: Can the turning point and end of an expanding epidemic be precisely forecast? arXiv preprint arXiv:2004.08842, 2020.
- [56] Alex Arenas et al. A mathematical model for the spatiotemporal epidemic spreading of covid19. medRxiv, 2020.
- [57] Andrea L Bertozzi et al. The challenges of modeling and forecasting the spread of covid-19. arXiv preprint arXiv:2004.04741, 2020.
- [58] HM Singer. Short-term predictions of country-specific covid-19 infection rates based on power law scaling exponents. arXiv preprint arXiv:2003.11997, 2020.
- [59] Matheus Henrique Dal Molin Ribeiro, Ramon Gomes da Silva, Viviana Cocco Mariani, and Leandro dos Santos Coelho. Short-term forecasting covid-19 cumulative confirmed cases: Perspectives for brazil. *Chaos, Solitons & Fractals*, page 109853, 2020.
- [60] Luis Orea, Inmaculada C Álvarez, et al. How effective has been the spanish lockdown to battle covid-19? a spatial analysis of the coronavirus propagation across provinces. Technical report, 2020.
- [61] Juan C Mora et al. A semiempirical dynamical model to forecast the propagation of epidemics: The case of

- the sars-cov-2 in spain.  $arXiv\ preprint\ arXiv:2004.08990,$  2020.
- [62] H. Ritchie *et al.* Coronavirus pandemic (covid-19), data repository. https://ourworldindata.org, 2020.
- [63] Steven H Strogatz. Nonlinear dynamics and chaos with student solutions manual: With applications to physics, biology, chemistry, and engineering. CRC press, 2018.
- [64] David Roxbee Cox and David Victor Hinkley. Theoretical statistics. CRC Press, 1979.
- [65] By definition  $e := \sqrt{1 (b/a)^2}$ , with a and b respectively the major and minor radiuses of a regular ellipse. in our case  $r_{max}$  and  $r_{\perp}$  play respectively the analogous roles of a and b for the plume-like epidemic trajectories, from which the expression in the main text follows.
- [66] Notice that the linear regression analysis yields an intercept  $r_0 \simeq -4.1$  which, in turns, means a proportionality factor  $\mathcal{A}_0 \simeq 10^{-4}$  between  $r_{max}$  and p, meaning a magnitude of  $\mathcal{T} \simeq 3.2$  for  $p \sim 10^5$ , and increasing to  $\mathcal{T} \simeq 6.3$  for  $p \sim 10^8$ .
- [67] Graziano Onder, Giovanni Rezza, and Silvio Brusaferro. Case-fatality rate and characteristics of patients dying in relation to covid-19 in italy. *Jama*, 323(18):1775–1776, 2020.
- [68] E Lee Daugherty Biddison, Ruth Faden, Howard S Gwon, Darren P Mareiniss, Alan C Regenberg, Monica Schoch-Spana, Jack Schwartz, and Eric S Toner. Too many patients? a framework to guide statewide allocation of scarce mechanical ventilation during disasters. *Chest*, 155(4):848–854, 2019.
- [69] Vitor E Valenti, Pedro de Lemos Menezes, Ana Carolina Gonçalves de Abreu, Gustavo Nakamura Alves Vieira, and David M Garner. Social distancing measures may have reduced the estimated deaths related to covid-19 in brazil. *Journal of Human Growth and Development*, 30(2):164–169, 2020.
- [70] Benedetta Armocida, Beatrice Formenti, Silvia Ussai, Francesca Palestra, and Eduardo Missoni. The italian health system and the covid-19 challenge. The Lancet Public Health, 5(5):e253, 2020.
- [71] Joseph T Wu, Kathy Leung, and Gabriel M Leung. Nowcasting and forecasting the potential domestic and international spread of the 2019-ncov outbreak originating in wuhan, china: a modelling study. *The Lancet*, 395(10225):689-697, 2020.
- [72] CDC Covid and Response Team. Severe outcomes among patients with coronavirus disease 2019 (covid-19)?united states, february 12-march 16, 2020. MMWR Morb Mortal Wkly Rep, 69(12):343-346, 2020.
- [73] Qifang Bi, Yongsheng Wu, Shujiang Mei, Chenfei Ye, Xuan Zou, Zhen Zhang, Xiaojian Liu, Lan Wei, Shaun A Truelove, Tong Zhang, et al. Epidemiology and transmission of covid-19 in shenzhen china: Analysis of 391 cases and 1,286 of their close contacts. *MedRxiv*, 2020.
- [74] Jesús Gómez-Gardenes, David Soriano-Panos, and Alex Arenas. Critical regimes driven by recurrent mobility patterns of reaction-diffusion processes in networks. Nature Physics, 14(4):391–395, 2018.
- [75] D Soriano-Paños, L Lotero, A Arenas, and J Gómez-Gardeñes. Spreading processes in multiplex metapopulations containing different mobility networks. *Physical Review X*, 8(3):031039, 2018.
- [76] Romualdo Pastor-Satorras, Claudio Castellano, Piet Van Mieghem, and Alessandro Vespignani. Epidemic processes in complex networks. Reviews of modern physics,

- 87(3):925, 2015.
- [77] Arghya Das, Abhishek Dhar, Anupam Kundu, and Srashti Goyal. Covid-19: analysis of a modified seir model, a comparison of different intervention strategies and projections for india. medRxiv, 2020.
- [78] Helmut Hlavacs. How often should people be tested for corona to avoid a shutdown? arXiv preprint arXiv:2004.14767, 2020.
- [79] Jorge Rodriguez, Mauricio Paton, Joao M Uratani, and Juan M Acuna. Modelling the impact of interventions on the progress of the covid-19 outbreak including age segregation. medRxiv, 2020.
- [80] Chintan Shah, Nima Dehmamy, Nicola Perra, Matteo Chinazzi, Albert-László Barabási, Alessandro Vespignani, and Rose Yu. Finding patient zero: Learning contagion source with graph neural networks. arXiv preprint arXiv:2006.11913, 2020.
- [81] Roy M Anderson and Robert M May. Infectious diseases of humans: dynamics and control. Oxford university press, 1992.
- [82] Herbert W Hethcote. The mathematics of infectious diseases. SIAM review, 42(4):599-653, 2000.
- [83] Jessica T Davis, Matteo Chinazzi, Nicola Perra, Kunpeng Mu, Ana Pastore y Piontti, Marco Ajelli, Natalie E Dean, Corrado Gioannini, Maria Litvinova, Stefano Merler, Luca Rossi, Kaiyuan Sun, Xinyue Xiong, M. Elizabeth Halloran, Ira M Longini, Cécile Viboud, and Alessandro Vespignani. Estimating the establishment of local transmission and the cryptic phase of the covid-19 pandemic in the usa. medRxiv, 2020.
- [84] Marco D'Arienzo and Angela Coniglio. Assessment of the sars-cov-2 basic reproduction number, r0, based on the early phase of covid-19 outbreak in italy. *Biosafety* and *Health*, 2020.
- [85] Jon Cohen and Kai Kupferschmidt. Countries test tactics in ?war?against covid-19, 2020.
- [86] Ned Stafford. Covid-19: Why germany?s case fatality rate seems so low. Bmj, 369, 2020.
- [87] Janice Hopkins Tanne, Erika Hayasaki, Mark Zastrow, Priyanka Pulla, Paul Smith, and Acer Garcia Rada. Covid-19: how doctors and healthcare systems are tackling coronavirus worldwide. *Bmj*, 368, 2020.
- [88] Daniel B Jernigan. Update: public health response to the coronavirus disease 2019 outbreak?united states, february 24, 2020. MMWR. Morbidity and mortality weekly report. 69, 2020.